Fibril Elongation by Aβ$_{17-42}$: Kinetic Network Analysis of Hybrid-Resolution Molecular Dynamics Simulations
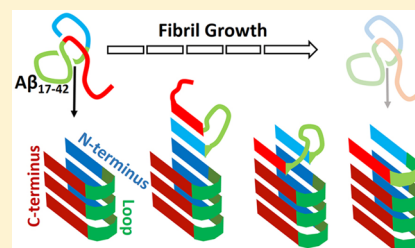
Wei Han[†,‡] and Klaus Schulten*[,†,‡,§]

[†]Beckman Institute, [‡]Center for Biophysics and Computational Biology, and [§]Department of Physics, University of Illinois at Urbana−Champaign, Urbana, Illinois 61801, United States

S *Supporting Information*

ABSTRACT: A critical step of β-amyloid fibril formation is fibril elongation in which amyloid-β monomers undergo structural transitions to fibrillar structures upon their binding to fibril tips. The atomic detail of the structural transitions remains poorly understood. Computational characterization of the structural transitions is limited so far to short Aβ segments (5−10 aa) owing to the long time scale of Aβ fibril elongation. To overcome the computational time scale limit, we combined a hybrid-resolution model with umbrella sampling and replica exchange molecular dynamics and performed altogether ~1.3 ms of molecular dynamics simulations of fibril elongation for Aβ$_{17-42}$. Kinetic network analysis of biased simulations resulted in a kinetic model that encompasses all Aβ segments essential for fibril formation. The model not only reproduces key properties of fibril elongation measured in experiments, including Aβ binding affinity, activation enthalpy of Aβ structural transitions and a large time scale gap ($\tau_{lock}/\tau_{dock} = 10^3 - 10^4$) between Aβ binding and its structural transitions, but also reveals detailed pathways involving structural transitions not seen before, namely, fibril formation both in hydrophobic regions L17-A21 and G37-A42 preceding fibril formation in hydrophilic region E22-A30. Moreover, the model identifies as important kinetic intermediates strand−loop−strand (SLS) structures of Aβ monomers, long suspected to be related to fibril elongation. The kinetic model suggests further that fibril elongation arises faster at the fibril tip with exposed L17-A21, rather than at the other tip, explaining thereby unidirectional fibril growth observed previously in experiments.

INTRODUCTION

Amyloid-β (Aβ) peptides having a length of 40−42 amino acids are naturally secreted as a cleavage product of the amyloid precursor protein.[1] Formation of Aβ aggregates in patient's brain is a hallmark of Alzheimer's disease.[2] Although the pathogenic identities and roles of Aβ aggregates are still under debate,[3] fibrillar aggregates formed by Aβ likely play a critical role in Aβ's cytotoxicity.[4−8] Inhibition of fibril formation may provide a potential means for reducing Aβ toxicity.[9,10]

Kinetic experiments have established that formation of Aβ fibrils include nucleation and elongation of fibrils.[11] After nucleation, Aβ monomers in solution are added to fibril tips to elongate fibrils. Kinetics of Aβ fibril elongation has been the subject of numerous experimental studies.[12−19] On the basis of the interpretation of kinetic data, these studies proposed a two-step "dock−lock" mechanism for fibril elongation: Aβ monomers in solution first dock quickly to fibril tips; then in a locking step, they undergo structural reorganization to assume fibril structures, probably with fibrils acting as templates.[13−16,18] It has been suggested that the locking step involving structural transitions of Aβ is likely the rate-limiting step.[13−16,18] Therefore, it is important to characterize, in molecular detail, not only various forms of Aβ, both in solution and in fibrils, but also kinetics of the structural transitions during fibril elongation. Such efforts could assist in the design of efficient inhibitors.

Significant progress has been achieved in the characterization of atomic structures of Aβ fibrils through solid-state NMR

experiments and modeling.[20−24] It is now known that Aβ fibrils mainly adopt cross-β structures which are rich in parallel, in-register β-sheets formed between peptides and aligned along the fibril axis. Though different in detail, the fibril models determined by several laboratories share a similar feature: there is a bending region located within residues 20−30 which brings into close contacts the two β-sheets adjacent to the bending region, providing additional stabilization to fibrils (Figure 1).[20−24] Furthermore, the models reveal an internal staggering between the two β-sheets, leading to structural distinction between the two fibril tips (Figure 1).[21,22] Similarly, structures of Aβ peptides in solution were also intensively characterized through a combination of solution NMR experiments and computer simulations, exhibiting an ensemble of heterogeneous, compact structures.[25−28] However, experimental information on structural transitions of Aβ during fibril elongation is still scarce except for the case of local conformational change of Aβ probed in a recent study combining two-dimensional ultraviolet spectroscopy and computer simulations.[29]

Complementary to experiment, molecular dynamics (MD) simulation has been a valuable tool to characterize the structural transitions involved in Aβ fibril elongation at various levels of detail.[30−41] A major challenge in simulating fibril
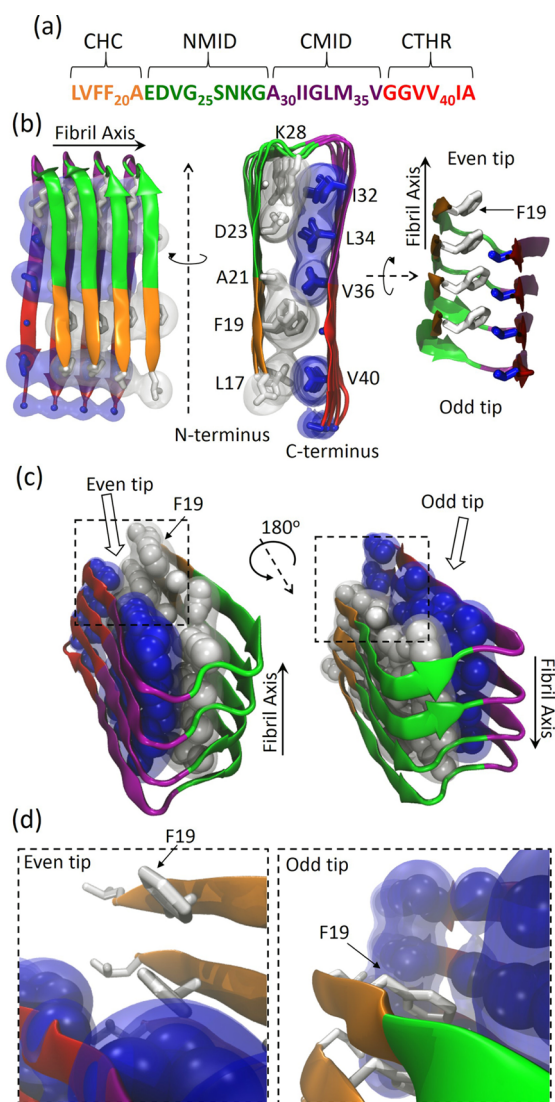
Figure 1. Cross-β structures formed by Aβ$_{17-42}$. (a) Amino acid sequence of Aβ$_{17-42}$ and definition of four regions, namely, CHC, NMID, CMID and CTHR, investigated in the present study. (b) Experimental fibril structures of Aβ$_{17-42}$ (PDB ID: 2BEG). Shown in orange, green, purple and red are the CHC, NMID, CMID and CTHR regions, respectively. The side chains wrapped in the fibril are shown in stick representation. Shown in gray and blue are the side chains in regions 17−26 and 31−42, respectively. Transparent ellipsoids depict the excluded volumes of the side chains. (c) Structural difference between even and odd fibril tip. All the side chains are shown in ball representation. In (b) and (c), the fibril axis points from the odd tip to the even tip. (d) Close-up view of fibril tip regions surrounding F19 as indicated by dashed boxes in (c).

elongation of Aβ arises from the slow elongation kinetics that requires ms to s long simulations to be reproduced.[16,18] To overcome this challenge, several coarse-grained (CG) models, which reduce the spatial resolution and thereby speed up simulations, have been employed to simulate Aβ fibril elongation starting with dissociated monomers, shedding light on the dock−lock mechanism of fibril elongation.[40,41] Despite some insight gained from the CG simulations, it is critical to model Aβ fibril elongation in atomic detail. All-atom simulations of Aβ fibril elongation are too daunting a task computationally. Fortunately, several short segments of Aβ, having length of 5−10 amino acids located within region K16-

A42, are experimentally known to form fibril by themselves.[24] For these segments, all-atom simulations of their fibril elongation become computationally practical, allowing observation in atomic detail of structural transitions arising in both the docking and locking steps.[33−37] An attempt has also been made in simulating docking of Aβ with fibril tips, revealing heterogeneous binding conformations.[38,39]

The observations of fibril elongation of short Aβ segments are intriguing and perhaps relevant to Aβ fibril elongation. However, considering that Aβ includes several aggregation-competent short segments and exhibits a complex architecture, the following questions regarding structural transitions during Aβ fibril elongation still need to be answered: (1) In which regions of Aβ do initial fibril contacts form? Is there any region of Aβ particularly favorable or unfavorable for initial fibril contacts? (2) Once initial fibril contacts form, how do fibril structures propagate through the remaining parts of Aβ? (3) Aβ, compared to the short segments, is supposed to exhibit more complex monomeric structures. What is the impact of these Aβ monomer structures on fibril elongation? (4) The intersheet staggering, which is seen in fibrils formed by Aβ, leads to the two tips of a fibril, the top and bottom tip, assuming actually different local structures.[21] Can the difference in the top and bottom tip lead to different fibril elongation kinetics and, thereby, account for unidirectional growth of Aβ fibrils as seen in experiment?[42,43]

Addressing these questions requires simulations probing dynamics on a long time scale. To achieve such computation, we employ here a hybrid-resolution model, namely, PACE,[44,45] which combines models at two resolutions, with proteins represented in a united-atom model and with solvent described in a coarse-grained solvent model, the MARITNI solvent.[46] PACE has been shown to accelerate simulations significantly while folding proteins into their native structures.[45,47,48] To enhance sampling, we also adopt an approach combining umbrella sampling and replica exchange molecular dynamics (REMD) employed in previous studies of protein−protein interactions[49] and aggregation.[37] Biased simulations are further used to construct a kinetic network by following previous studies on folding and conformational transitions of proteins.[50,51] The resulting kinetic network allows us to identify transition pathways using the recently developed transition path theory.[52,53]

By combining PACE, enhanced sampling and transition path theory, we determine ensembles of pathways and, thus, establish the kinetics of structural transitions of Aβ$_{17-42}$ during fibril elongation at both fibril tips. Rate analysis on the pathways reveals that formation of fibril structures by Aβ$_{17-42}$ indeed arises through a dock−lock mechanism. The pathways leading to formation of fibril structures reveal that hydrophobic regions L17-A21 and, to a lesser extent, G37-A42 exhibit a particular propensity for initial fibrillar contacts, consistent with previous all-atom simulation studies showing that region 16−22 is key to fibril formation.[34] We find that hairpin-like structures formed in monomers, similar to those observed in previous simulations,[28,54−56] are dominant on-pathway intermediates arising upon the initial fibrillar contacts. We further find that due to the local U-shape structures of fibrils and the need to unfold the prior hairpin-like structures of monomers, fibril structures propagate to the remaining parts of Aβ not in the expected zipper fashion, namely, do not propagate immediately to the parts adjacent in sequence to the initial contacts. Finally, comparison of the results of fibril elongation at the two
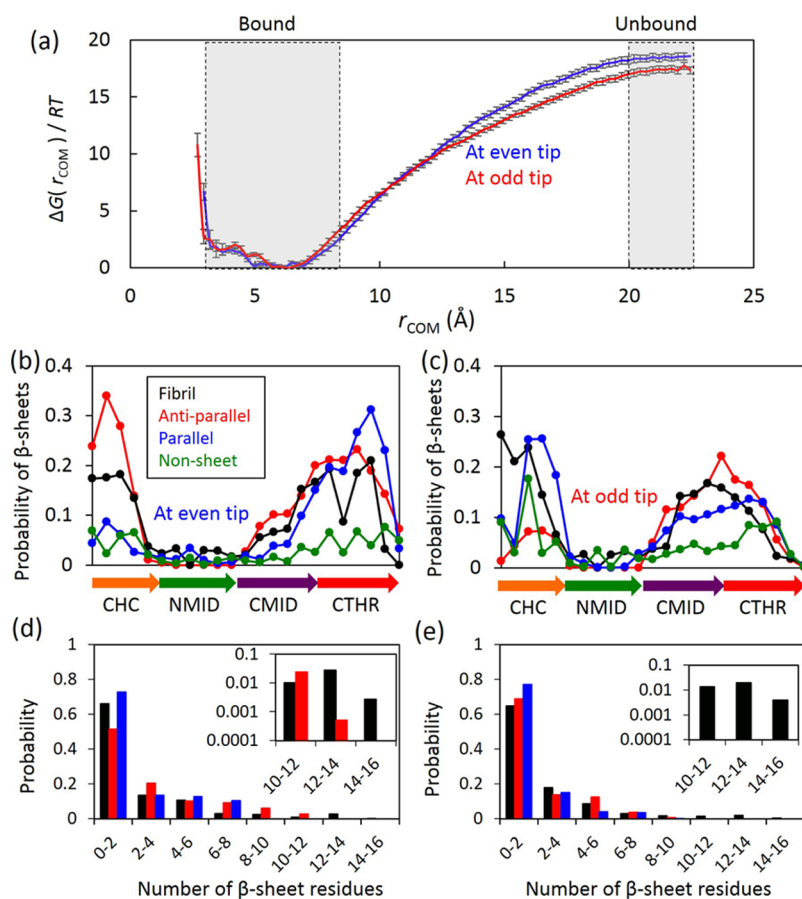
12451

dx.doi.org/10.1021/ja507002p | *J. Am. Chem. Soc.* 2014, 136, 12450−12460

Figure 2. Thermodynamics and structures in the docking step of fibril elongation. (a) Potential of mean force (PMF) profiles of docking of Aβ to even (blue) and odd (red) fibril tips. Error bars denote the difference between the PMFs calculated from two halves of simulations. (b,c) Residual probability of edge residues at even (b) and odd (c) tips forming fibrillar β-sheets (black), antiparallel β-sheets (red), parallel, out-of-register β-sheets (blue) and other structures involving hydrogen bond interactions (green). (d,e) Distributions of the numbers of edge residues at the even (d) and the odd (e) fibril tip forming fibrillar β-sheets (black), antiparallel β-sheets (red) and parallel, out-of-register β-sheets (blue). Shown in insets are close-up views of the distributions.

structurally different fibril tips suggests that the observed unidirectional growth of Aβ fibrils is mainly due to distinct growth rates at the two tips. The above findings not only provide experimentally testable predictions regarding fibril growth, but also reveal important details needed for modeling fibril growth at the level of overall kinetics.[57,58]

■ RESULTS

The present study focuses on fibril elongation of Aβ17−42. To investigate the roles of different parts of Aβ in fibril elongation, the peptide is divided into four regions (Figure 1a), including the central hydrophobic region (CHC, residues L17-A21), the C-terminal hydrophobic region (CTHR, G37-A42) and the N- and C-terminal parts of the middle region (NMID, E22-A30 and CMID, I31−V36). The fibril structures employed are the ones determined by Lührs et al. (Figure 1b) as a model for fibrils.[21] This model exhibits the U-shaped, cross-β structures usually seen in Aβ fibrils. Two β-sheets in the model, involving regions 17−26 and 31−42, form intersheet packing through side-chain contacts. Interestingly, due to the internal staggering of the two β-sheets, region 17−26 of a monomer forms side-chain contacts mostly with region 31−42 of the adjacent monomer, rather than with the region of the same monomer (Figure 1b). As a result, at the fibril tips one of the two regions, namely, region 17−26 or region 31−42, is left unpaired, leading

to two structurally different tips, namely, one (called even tip) with its CHC region (part of 17−26) exposed and the other (called odd tip) with its CHC region buried (see Figure 1c). We note that the geometry involved makes it impossible for an even tip to become an odd tip and vice versa; one end of a fibril sports an even tip throughout elongation, the other always an odd tip.[21]

In the following sections, we present first simulation results of the binding of Aβ monomers to both fibril tips. We compare then the kinetics, through kinetic network analysis, of the binding and actual formation of Aβ fibril structures, the latter process leading to fibril elongation. We further present the identified pathways and associated kinetics of structural transitions during fibril elongation at both tips and compare then the elongation kinetics. Finally, we discuss the possible factors that cause distinct kinetics at the two tips.

Aβ Docks to Fibrils with High Affinity while Assuming Heterogeneous Structures. To investigate the docking of Aβ monomers to fibril tips during fibril elongation, we first characterize the thermodynamics of Aβ docking. By definition,[13,14] the docking step involves binding of Aβ monomers to fibril tips irrespective of the detailed conformation that the Aβ monomer assumes in the process. Thus, the center-of-mass (COM) distance, r_{COM}, between Aβ monomers and fibril tips was chosen as the reaction coordinate for docking. On the basis

of biased simulations (see Methods), we calculated the potential of mean force (PMF) profiles with respect to r_{COM} for binding of Aβ monomers to both fibril tips, namely, the even and odd tip, at 332 K by means of the temperature-weighted histogram analysis method (T-WHAM).[59] The resulting PMFs, as shown in Figure 2a, are flat at large COM distances ($r_{COM} > 20$ Å), gradually decrease when the monomers are approaching the fibril tips and, eventually, exhibit a wide well at short distances (3 Å < r_{COM} < 8 Å) corresponding to the binding of monomers to the fibril tips and revealing actually a strong thermodynamic driving force of association. The binding affinities of Aβ monomers, converted to standard concentration conditions (see Supporting Information (SI)), were calculated to be be -19.4 ± 0.5 RT and -18.3 ± 0.6 RT for the even and the odd tip, respectively; the affinities are stronger than, but still comparable to, the value (-15.1 RT) derived on the basis of the critical concentration of soluble Aβ in equilibrium with fibrils.[15] Interestingly, the PMFs for the two tips are quite similar and the binding affinities differ only by about 1 RT. Energetic analysis reveals further that the binding between monomers and the even and the odd tip exhibits binding energies that are not significantly different (-113 ± 7 vs -112 ± 7 kcal/mol) and involves the burial of almost the same amount of hydrophobic surface area (1450 ± 70 vs 1460 ± 70 Å^2). Taken together, the simulations suggest that the structural difference between the two tips does not cause significantly different binding for Aβ.

Despite the observed large affinities of Aβ monomers in the docking step, the simulations show that fibril structures are usually not formed in this step, as revealed by the analysis of β-sheet structures formed between Aβ monomers and fibril tips (see SI). In general, there is a significant chance (40−70%) for β-sheets to form between monomers and most of the residues on the accessible edges of fibril tips, except for those located in the NMID region (Figure 2b,c). Each of these residues can be involved in various types of β-sheet, such as parallel, in-register β-sheet seen in actual fibrils and out-of-register β-sheet arranged either in antiparallel or parallel fashion; none of the mentioned β-sheet types appear to be dominant during in the monomer bound states (Figure 2b,c). As individual residues have a considerable probability, usually 10−25%, of being involved in either type of β-sheet, one wonders whether it is possible for uniform β-sheet structures to arise in monomer-bound states. To address this possibility, all monomer-bound states were binned according to the number of edge residues involved in the same type of β-sheet. The results suggest that in most cases at most six edge residues can be involved simultaneously in the same type of β-sheet (Figure 2d,e). Uniform β-sheet structures are rarely seen except for fibril β-sheet arising at both fibril tips with a probability of 2−3%; antiparallel β-sheet arises only at the even tip with a probability of 2% (insets, Figure 2d,e).

Our results are consistent with experimental kinetic studies, which suggest that Aβ monomers docking to fibril tips assume a wide spectrum of structures, including both fibrillar and disordered conformations.[18] The fully formed fibril structures observed here, though exhibiting only a small probability, could still serve as templates to incorporate additional Aβ monomers. In the present study, we simulated only the binding of single monomers to existing fibrils, the process of incorporating additional monomers was not simulated. We suspect that in reality the observed fully formed fibrillar structures, arising with

small probability, convert further other monomers into fibrillar structures, leading eventually to irreversible fibril formation.

Structural Transitions Leading to Fibril Elongation at the Even Tip. To characterize the structural transitions of Aβ leading to fibril elongation, we constructed from about 2.1×10^6 conformations sampled in the biased simulations, as described in Methods and SI, a kinetic network model constituting about 10^5 microstates. Employing transition path theory (TPT, see Methods)[52,53] the network model was decomposed into microscopic transition pathways that identify routes from soluble states ($r_{COM} > 20$ Å) to fibrillar states, the latter involving at least 12 edge residues in fibrillar β-sheets. The decomposition analysis identified a large number of pathways, each involving 20−39 intermediate states. The most populated 26 pathways account for only ∼50% of reactive transitions. These pathways are heterogeneous, as revealed by their projection on the first two most significant principle components arising from the principal components analysis described in SI (Figure 3).
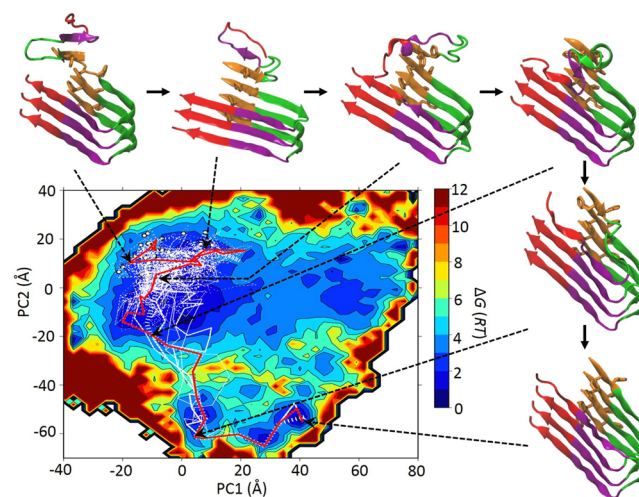

Figure 3. Pathways of fibril elongation identified at the even tip. The major pathways (white lines) accounting for 50% of transitions and their starting points (white dots) were projected onto the potential of mean force (PMF) profile (colored contour map) with respect to the first two principal components (PC1 and PC2), namely, those with the two largest eigenvalues, obtained through principal component analysis (PCA) based on a covariance matrix of 625 C$_\alpha$−C$_\alpha$ distances between the incoming monomer and the fibril even tip and 231 C$_\alpha$−C$_\alpha$ distances within the monomer (see SI). PC1 and PC2 account for 54% of total variance in the distances used in the PCA. The PMF was calculated at 332 K using the T-WHAM method.[59] The most populated pathway is highlighted by a red line. Shown are also select intermediates of this pathway; represented in orange, green, purple and red are the Aβ CHC, NMID, CMID and CTHR regions, respectively. The locations of the intermediates in the pathway are indicated by dashed arrows.

To gain insight into the elongation mechanism represented by the pathways we simplified the pathways by grouping them according to the order of formation of β-sheet structures in different regions of Aβ (see SI). The simplified pathways, as summarized in Figure 4, reveal that in the majority (∼97%) of transition pathways fibril structures start to arise in the CHC region (Figures 1 and 3), while in some (38%) of these pathways formation of antiparallel β-sheets in this region precedes formation of fibril structures (Figure S1a (SI)). The
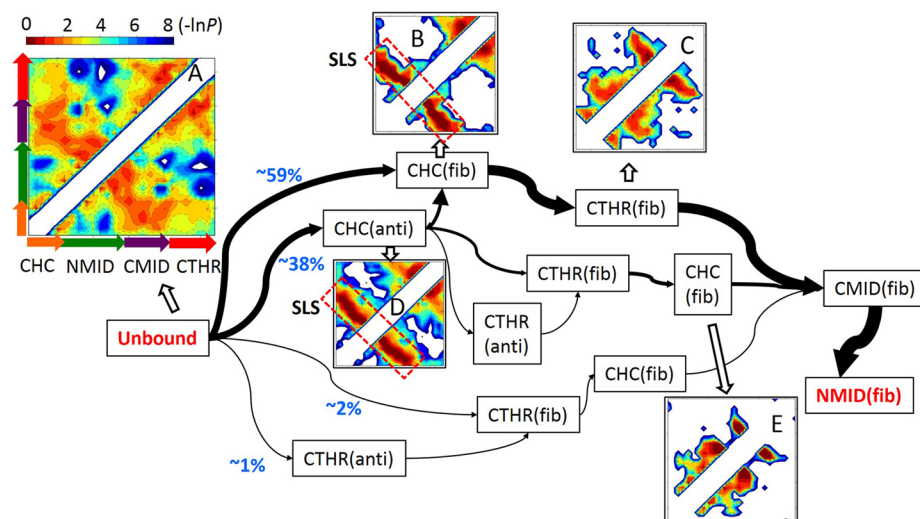
Figure 4. Simplified network of fibril formation during fibril elongation at the even tip. The network was generated (see SI) on the basis of the order of β-sheet formation in four regions, namely, CHC, NMID, CMID and CTHR. Shown as text boxes are all the intermediates where either antiparallel ("anti") or fibrillar ("fib") β-sheets form in one of the four regions. Black arrows denote fluxes of reactive transitions with the arrow thickness proportional to the probabilities of the transitions. The percentage numbers in blue denote the probability of initial transitions. Following any path connecting boxes "Unbound" and "NMID(fib)" yields a possible sequence of β-sheet formation observed in the present study. The five color maps shown nearby the network represent the probabilities (P) of inter-residual contact within the incoming monomer at different stages of fibril formation, including unbound states (A), initial contact states (B and D) and states where fibril structures form both in the CHC and CTHR regions (C and E). The probability of contact between residues i and j within the incoming monomer was calculated as the probability of C_α atoms of the two residues being within a cutoff of 6.5 Å, averaged over all states that belong to the same stage of fibril formation. The axes of map A are shown as a chain of orange, green, purple and red arrows, which denote the positions of regions CHC, NMID, CMID and CTHR on the map, respectively. All residual contact probabilities (P) are scaled as $-\ln P$. The color bar on the top of map A denotes the $-\ln P$ scale in units RT. Maps B−E have their corresponding axes and color bar removed. The red dashed boxes in the maps indicate the contact patterns of the incoming monomer that exhibits the strand−loop−strand structures (SLS).

transitions from the antiparallel to fibrillar β-sheets in the CHC region appear to be similar to the antiparallel ↔ parallel transitions observed in previous MD studies of Aβ$_{16-22}$ dimers,[60] arising through rotation of the CHC region of a monomer about a hydrogen bond (HB) formed between the amide hydrogen of F19 in the monomer and the carbonyl group of V18 at the even tip (Figure S1b (SI)). In subsequent steps, the fibril structures extend to the CTHR region, then to the CMID region, and finally to the NMID region. Beside the major transition pathways, there is a small chance that extension of the fibril structures follows a slightly different pathway in which structures are formed initially in the CTHR region and then propagate to the CHC region (Figure 4). The chance of these minor pathways is low (~3%) at 332 K, but increases to ~14% at high temperature (370 K) (Figure 5a).

In all the pathways analyzed the fibril structures are initiated either in the CHC region or, to a lesser extent, in the CTHR region, but never in the middle regions (NMID and CMID) of Aβ (Figure 4). One wonders whether this result arises from a bias introduced by the enhanced simulations used here for the network analysis. To address this question, we performed, as described in Methods, multiple 100 ns unbiased simulations of the association of Aβ with the fibrils. Although it is unlikely to observe the formation of fibril conformations on such a short time scale, the formation of initial HB contacts between monomers and the even fibril tip indeed occurred in a large number (164) of simulations. If initial HB contacts form randomly, the chance to observe the formation of HB between a specific pair of residues of monomers and fibril tips is roughly $1/25^2 = 0.16\%$ for Aβ$_{17-42}$. On the basis of this probability, we estimated for each region of Aβ the expected numbers of
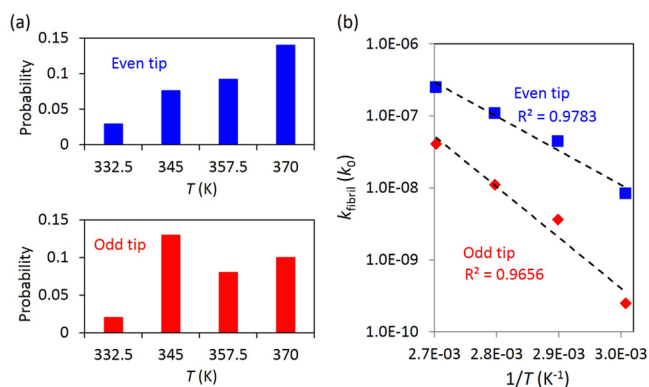

Figure 5. Temperature dependence of kinetics of fibril formation at both fibril tips. (a) Probabilities of pathways initiated with formation of fibril structures in the CTHR region during fibril elongation at the even and the odd tip. (b) Temperature dependence of fibril formation at the even and the odd tip. Rates were fitted to the Arrhenius relationship (eq 1) with fitting quality R^2 shown nearby.

trajectories in which at least one fibrillar HB could form in this region (Figure 6a). Our simulations show that the NMID and CMID regions are highly unfavorable for initial fibril contacts while the CHC and CTHR regions are involved in initial fibril contacts more frequently than expected on average. In particular, the trajectories leading to fibril formation in the CHC region are six times more frequent than the mere average. Altogether, our simulations suggest that formation of initial fibril contacts is sequence-specific and favorable in the hydrophobic regions.
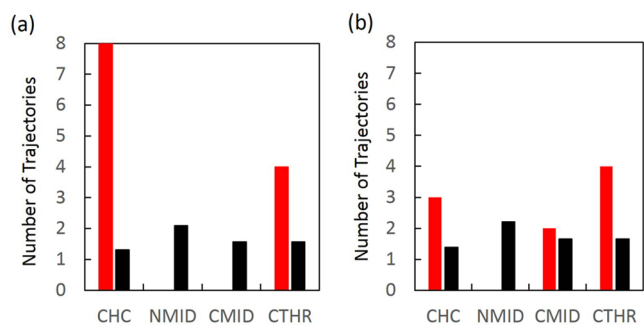
Figure 6. Comparison between number of standard simulations in which fibril contacts arise (red bars) and expected numbers of simulations in which initial fibril contacts form randomly (black bars) at the even (a) and the odd tip (b). The expected numbers for any region were estimated as the number of simulations observed to form a contact × the number of residues in this region × $1/25^2$.

Strand−Loop−Strand Structures of Aβ Monomers Essential for Fibril Formation. In the process of fibril elongation, the incoming monomers need to bind to the tip, but also need to undergo conformational transitions. To characterize the conformational transitions, we monitored structural features of a monomer at different stages of fibril formation, carrying out cluster and contact analysis of monomer trajectories. The cluster analysis of unbound monomers ($r_{COM} > 20$ Å) (Figure S2 (SI)) shows that these monomers adopt heterogeneous structures, the most populated five of which account for only ∼20% of total populations. The tertiary structures of the monomers were further examined by monitoring contact maps of backbone C_α atoms of a monomer, using a 6.5 Å distance cutoff for contacts. Two major types of tertiary contacts emerge from the contact map (A in Figure 4), one formed between the CHC and CMID regions and the other formed between the CMID and CTHR regions, both consistent with previous all-atom MD studies.[26,61]

When initial fibrillar contacts form in the CHC region, the monomer tends to adopt hairpin-like structures involving antiparallel contacts between the CHC and CMID regions and a reversed loop spanning the NMID region, as revealed by the corresponding contact maps (B and D in Figure 4) showing an off-diagonal band of high contact probabilities spanning residues 17−36. These structures, known as strand−loop−strand (SLS) structures (Figure S3a (SI)), have been suggested both in experimental and theoretical studies as important monomer intermediates for fibril elongation.[28,54−56,62] To quantify the involvement of the strand−loop−strand (SLS) structures in fibril elongation, we calculated, as described in SI, the probability (p_{onpath}) of the SLSs being present in the transition pathways. The on-pathway probability of SLSs turns out to be ∼53%, much higher than the probability (∼10−13%) for either unbound or bound monomers to adopt the SLSs, suggesting, therefore, that the SLSs are indeed important intermediates for monomers during fibril elongation.

Eventually, the monomer loses most of its internal contacts involved in the SLSs when fibril structures have been achieved in the CHC and CTHR regions (B → C and D → E in Figure 4). The simulations suggest that the SLSs need to be disrupted for fibril structures to extend, often prior to fibril contact extension to the middle regions (NMID and CMID) of Aβ.

Rate of Fibril Formation at Even Tips. Of great practical concern regarding fibril formation are the rates of elongation kinetics. In order to determine the rates we performed the

network analysis as described in Methods on the constructed kinetic network to estimate the macroscopic rate of transitions from soluble Aβ ($r_{COM} > 20$ Å) to either bound or fibrillar forms of Aβ, the former representing the docking transitions and the latter representing the actual elongation of fibrils. The rates of the two types of transitions (Table 1) were calculated

Table 1. Rates of the Docking Step (k_{dock}) and Formation of Fibril Structures in the CHC Region (k_{CHC}) and in the Entire Aβ (k_{fibril}) at the Even and Odd Fibril Tips[a]

	k_{dock}	k_{CHC}	k_{fibril}
even tip	∼3 × 10^{-5}	∼3 × 10^{-8}	∼8 × 10^{-9}
odd tip	∼2 × 10^{-5}	∼6 × 10^{-9}	∼2 × 10^{-10}

[a]All rates were calculated at 332 K. The calculation procedure is described in SI. The rate values reported in this table are given in terms of a reduced unit of k_0, the base rate constant used to estimate transition rates in rate matrices. A rough estimate suggests $k_0 \approx (20$ ps$)^{-1}$ (see SI).

to be ∼3 × $10^{-5}k_0$ and ∼8 × $10^{-9}k_0$, respectively, where k_0, as described in SI, is a base rate constant for the network. The time scales of the docking transitions and fibril elongation were thus estimated to be ∼0.5 μs and ∼2−3 ms, respectively, revealing a large time scale gap (10^3−10^4) between the two transitions.

Our kinetic network analysis revealed a complex energy landscape governing multitime scale processes involving fibril elongation. One may wonder whether fibril elongation corresponds to the slowest kinetic process of the fibril-monomer system. To address this question, the relaxation rates k of the slowest kinetic processes were estimated by calculating the smallest (in terms of magnitude) nonzero eigenvalues λ of the rate matrix associated with the kinetic network and employing then the relationship $k = -\lambda$.[63] The calculation revealed that the rates of the eight slowest relaxation modes range from ∼8 × $10^{-13}k_0$ to ∼8 × $10^{-10}k_0$, all smaller than k_{fibril} (∼8 × $10^{-9}k_0$). Apparently, fibril elongation is not one of the slowest transition processes that the fibril-monomer system undergoes.

Aβ elongation kinetics is known to follow the Arrhenius law

$$k = Ae^{\Delta H^{\ddagger}/RT} \tag{1}$$

where A is a pre-exponential factor and $\Delta H^{\ddagger}$ is the activation enthalpy.[12,17] It has been shown that Aβ elongation exhibits a large positive activation enthalpy ($\Delta H^{\ddagger}$), indicating a significant structural reorganization arising during fibril growth.[12,17] Therefore, it is essential to examine the temperature dependence of the kinetic model derived for formation of fibril structures. For this purpose, the network models were reconstructed at various temperatures based on the same biased simulations using T-WHAM.[59] The rates of fibril formation (k_{fibril}) at 332−370 K obtained thus agree well with the Arrhenius law, exhibiting a fitting correlation coefficient R^2 = 0.98 (Figure 5b). The activation enthalpy $\Delta H^{\ddagger}$ extracted from the fitting is ∼22 kcal/mol, higher than, but still comparable to, the value (∼15.8 kcal/mol) reported for Aβ$_{1−42}$ obtained through quartz crystal microbalance measurements.[17] The large activation enthalpy obtained is consistent with the large structural reorganization of monomers observed in our kinetic model (Figure 4).

Fibril Elongation at Odd Tip Is Kinetically Unfavorable. To identify the difference in kinetics between fibril
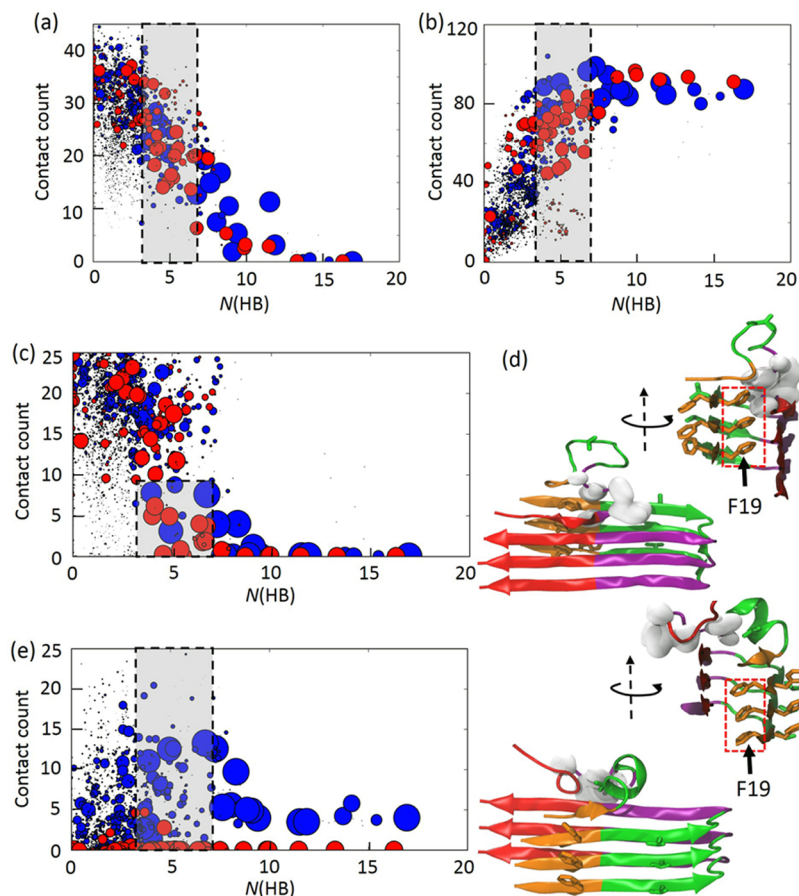
Figure 7. Losses and gains of contacts for the incoming monomer during formation of fibril structures. (a) Plot of the number of internal residual contacts of the monomers against the number of hydrogen bonds (N_{HB}) formed between monomer and fibril tips for all on-pathway intermediates. (b) Plot of the number of side chain contacts formed between monomer and fibril tips against N_{HB}. (c) Plot of the number of internal contacts of the monomer formed between L17-A21 and I31-V36 against N_{HB}. The shaded region highlights the states in which the monomer involves only about five HBs with the fibril tip but loses most of its internal contacts. (d) Representative structures of major intermediates of fibril elongation at the even (top) and the odd (bottom) tip as highlighted in the shaded region in panel (c). Shown in orange, green, purple and red are the CHC, NMID, CMID and CTHR regions, respectively. The side chains of F19 and F20 are shown in stick representation. The side chains of I31-V36 in the monomer are shown as white ellipsoids. (e) Plot of the number of side chain contacts formed between I31−V36 of the monomer and F19 of the fibril against N_{HB}. In panels (a−c) and (e), the intermediates arising from fibril elongation at the even and the odd tip are plotted as blue and red circles, respectively, with the radii of circles proportional to $-\ln p_{\text{onpath}}$. The shaded regions in (a), (b) and (e) denote the stages where drastic change of contacts arises.

elongation at the even and the odd fibril tip, the network analysis applied for fibril elongation at the even tip was also applied to investigate fibril elongation at the odd tip. The pathway analysis revealed that the elongation at the even and the odd tip proceed largely in a similar manner in regard to the order in which monomer regions attach to fibrils (Figures S4 and S5 (SI)). At 332 K, in most pathways (∼98%), the fibril structures are initiated in the CHC region and then extend to the CTHR and CMID regions (Figure S5 (SI)). In minor pathways (∼2%), the fibril structures start either in region CTHR or CMID and extend then to the CHC region (Figure S5 (SI)). The probability of the minor pathways increases (8−13%) at elevated temperature (345−370 K) (Figure 5a). In addition, the strand−loop−strand structures for the incoming monomer appear to a major degree (∼89%) on-pathway (Figure S3b (SI)). However, despite the similarity observed, the formation of fibril structures was found to be about 40 times slower at the odd tip than at the even tip (Table 1). Moreover, the corresponding activation enthalpy $\Delta H^{\ddagger}$, estimated to be ∼34 kcal/mol (Figure 5b), is much higher

than that for fibril growth at the even tip (∼22 kcal/mol). Taken together, our results suggest that fibril elongation at the odd tip is kinetically unfavorable.

Factors That Slow down Fibril Elongation at the Odd Tip. To find out what causes slower fibril elongation at the odd tip, kinetics of fibril formation in the CHC region was first investigated as this region was found to be key for the initial fibril elongation step at both tips. Since the CHC region of the fibril edge is highly exposed at the even tip, but partially shielded at the odd tip (Figure 1b), it is possible that initial fibril formation in the CHC region is hindered at the odd tip. To examine this possibility, we compared the rates (k_{CHC}) of formation of fibril structures only in the CHC region at both tips (Table 1). The comparison showed that the fibril structures in the CHC region arise about five times more slowly at the odd tip than they do at the even tip. Moreover, out of 173 unbiased simulations in which HBs formed between monomers and the odd tip, only three showed the formation of fibrillar HBs in the CHC region, which is less often than found (8 out of 164) in the simulations of Aβ binding to the even tip (Figure

6). Taken together, the less accessible CHC region at the odd tip does account, though only partially, for the slower formation of fibril structures at this tip.

Apart from initial fibril formation, the subsequent structural transitions of monomers were also investigated. The detail of the transitions of the monomer were examined by monitoring the monomer's internal contacts and its contacts with fibrils for all intermediates in the pathways to fibril formation, employing the number of hydrogen bonds formed between the monomer and the fibrils as the reaction progress variable. At early stages of the elongation at both tips ($N_{HB} = \sim 5$) the monomer loses most (∼70%) of its internal contacts (Figure 7a), mainly due to the loss of contacts in region L17-V36 where the strand−loop−strand (SLS) structures form (Figure 7c). In the meanwhile, considerable side chain contacts between the monomer and the fibrils arise, presumably compensating the loss of contacts in the monomer (Figure 7b). Moreover, there are more contacts formed at these early stages ($N_{HB} = \sim 5$) during the transitions arising at the even tip than at the odd tip (Figure 7b).

To examine why more contacts are formed for the transitions at the even tip, we inspected the intermediates arising at this early stage highlighted by the shaded region in Figure 7c. The structures of the intermediates reveal that the CMID region of the monomer forms contacts with side chains of F19 located at the even tip. The same contacts are absent in the intermediates arising at the odd tip (Figure 7d). These contacts were further monitored during the entire course of fibril formation (Figure 7e). The analysis shows that for fibril elongation at the even tip the contacts gradually increase at the early stage ($N_{HB} < 5$), coincident with the loss of internal contacts of the monomer, but vanish after considerable HB interactions ($N_{HB} > 10$) between the monomer and the fibril arise. The same contacts, on the other hand, do not arise throughout fibril formation at the odd tip. Therefore, our results suggest that the exposed side chains of F19 at the even tip may transiently stabilize the disrupted structures of the monomer and, thereby, facilitate formation of fibril structures.

■ DISCUSSION AND CONCLUSION

In the present study, we thought to describe Aβ fibril elongation[30] in atomic detail. To this end we performed molecular dynamics (MD) simulations of fibril elongation by $A\beta_{17-42}$. To overcome difficulties in simulating slow fibril elongation, both a hybrid-resolution model[44,45,48] and an enhanced sampling method combining umbrella sampling and REMD were employed. Kinetic network analysis[50,51,53] was then applied to furnish a kinetic model for fibril elongation, allowing us to identify structural transitions of Aβ involved in fibril elongation.

The "dock−lock" mechanism for fibril elongation proposed earlier on the basis of experiments[13,16,18] has received support from numerous MD studies focusing on fibril elongation by short Aβ segments, including $A\beta_{16-22}$, $A\beta_{15-28}$, $A\beta_{35-40}$ and $A\beta_{37-42}$.[34−37] The kinetic model derived in the present study reveals that fibril elongation by $A\beta_{17-42}$, which comprises basically all residues essential for fibril formation,[21] also follows this mechanism. Moreover, our rate calculation (Table 1) reveals a large time scale gap ($\tau_{lock}/\tau_{dock} = 10^{3-4}$) between the dock (docking of monomer to fibril tip) and the lock (conformational transition of monomer to fibril structure) steps. Our result agrees well with recent kinetic experiments by Qiang et al., who showed that the measured rate of fibril elongation for full-length Aβ is ∼10^4 times slower than

expected for fibril growth by diffusion-limited attachment of monomers to fibril tips.[18] Notably, the time scale gap calculated for $A\beta_{17-42}$ is much larger than that ($\tau_{lock}/\tau_{dock} \sim 10$) for a short segment like $A\beta_{16-22}$ as reported in previous simulations,[34] suggesting that the length of Aβ segments has a profound effect on separating the time scales of the docking and locking steps during fibril elongation.

The fibril formation pathways identified in the present study reveal that different regions of Aβ vary in their involvement in initial fibril formation. In particular, the NMID region (E22-A30) does not participate in initial fibrillar contacts (Figures 4, 6 and S5 (SI)). The following factors seem to contribute to the lack of involvement of the NMD region. One factor is that the NMID region includes largely polar and charged amino acids which may incur desolvation penalty against association; in fact, previous all-atom simulations of Aβ fibrils have shown that the same region of fibril edges gradually leaves fibrils driven by solvation.[64,65] The second factor is that the NMID region adopts tight loop structures and appears to be the most structured part of the peptide according to both NMR experiments[66] and simulations of Aβ monomers by others[26,54,67] as well as those in the present study. Involvement of the NMID region in fibril formation would be highly unfavorable as it requires disruption of the loop structures formed in this region. In contrast, initial fibril formation in the CHC region is more favorable compared to the other regions, highlighting the important role of the hydrophobicity of CHC in driving initial fibril formation.

The analysis based on energy-landscape theory by Massi and Straub proposed that certain conformations of monomers could undergo little structural reorganization upon binding to fibrils, thereby serving as important intermediates for fibril elongation.[31] Several experimental[28,62,68] and computational studies,[28,54−56] in seeking such intermediates, discovered monomeric structures in a hairpin-like motif of residues 16−35, called strand−loop−strand (SLS) motif. On the basis of their structural resemblance with the U-shape topology of Aβ seen in fibrils, the SLS structures have been proposed to be important intermediates for fibril elongation.[28,54−56,62,68] Our simulations show that the SLS structures arise in a majority (∼50−90%) of the identified pathways when the initial fibrillar contacts are formed in the CHC region. On the one hand, this finding provides direct support to the notion that the SLSs are on-pathways intermediates in fibril elongation as suspected previously; on the other hand, the hydrogen bonds formed within the SLS structures need to also be broken to allow other parts of peptides to participate further in hydrogen bonds with fibrils. The breaking of the SLS structures could be energetically unfavorable, as indicated by a large positive activation enthalpy (∼22 kcal/mol) of fibril elongation estimated in the present study, comparable to that (∼15.8 kcal/mol) reported in kinetic experiments.[17] Interestingly, a similar conclusion regarding the role of hairpin-like monomeric intermediates in fibril growth has also been reached in a previous all-atom study for a shorter segment, namely, $A\beta_{25-35}$.[69]

The key role of SLSs in fibril elongation raises the possibility that the SLS structures can serve as a target for fibril inhibition. Destabilizing SLS formation in Aβ or preventing Aβ with the SLS structures from binding to fibrils may slow down fibril formation. Despite the significant involvement of the SLS structures in fibril formation, our results do indicate a non-negligible chance of fibril formation which does not rely on SLSs and, thereby, may not be affected by inhibiting SLSs.

Therefore, it remains an open question how effective the SLS structures are as an inhibition target.

It has been assumed that after the initial contact, fibril structures propagate immediately to the regions adjacent in sequence to the initial contacts.[58] Indeed, this assumption has been supported by all-atom simulations of fibril elongation by short Aβ segments like Aβ_{16-22},[34] Aβ_{35-40}[37] and Aβ_{37-42}.[36] If the same assumption is also true for Aβ_{17-42}, one would expect that fibril structures extend to the middle regions (NMID and CMID) after the initial contact form in region CHC or CTHR. Our simulations reveal instead that once fibril contacts are initiated in either region CHC or region CTHR, the structures continue to arise mainly in the other of the two regions (Figures 3 and S5 (SI)). The fibril structures in the NMID region are the last to arise. Regions CHC and CTHR, though distant in sequence, are spatially close to each other in the U-shaped fibril structures (Figure 1). Thus, fibril extension in the way stated above may allow the monomer to maintain at least partly its hairpin-like structures arising upon the initial contacts (Figure 3). On the other hand, if fibril structures extend to the NMID region as expected, the loop of the hairpin-like structures would participate in fibril formation, leading immediately to deformation of the entire hairpin-like structures.

Our results disagree with the Aβ locking mechanism suggested on the basis of a coarse-grained MD study.[41] According to this mechanism, when a monomer makes initial fibrillar contact with one of the two β-sheets in fibrils, the remaining part of the monomer still moves freely and, thus, fibrillar contacts can propagate along the remaining part of the monomer.[41] Instead, the route of fibril extension observed in the present study agrees with a transition state ensemble model for Aβ fibril elongation as reported recently on the basis of all-atom simulations.[35] The reported model, derived indirectly through unfolding simulations of Aβ fibril structures, develops intact fibril contacts in the hydrophobic regions of both β-sheets of fibrils, but exhibits disordered loops in the NMID region. During fibril elongation, such transition states could be reached by unbound Aβ monomers only if their conformational transitions to fibril structures follow a route similar to the one observed in the present study.[35]

Aβ fibrils are known to grow unidirectionally.[42,43] Structural characterization of Aβ fibrils reveal distinct structures of two fibril tips exposing either their N-terminal or C-terminal edges (Figure 1), indicating different binding interfaces for incoming monomers.[21] Previous all-atom simulations aiming to link this finding with unidirectional fibril growth suggested that Aβ peptides bind to the two fibril tips with different affinities.[39] In contrast, a computational study employing coarse-grained (CG) models showed that Aβ monomers bind to either fibril tip without apparent thermodynamic preference.[41] Moreover, another CG simulation study proposed that the fibril tip with its CHC region more accessible can allow faster formation of initial fibril structures and, thereby, facilitates fibril growth at this tip.[40] In the present study, we found that Aβ binds to the two fibril tips with similar affinities, but that fibril structures form much faster (about 40 times) at the tip exposing the CHC region (even tip) than they do at the other tip (odd tip). Our analysis revealed that the exposed CHC region at the even tip indeed promotes initial fibril formation as suggested in previous studies. However, this promotion contributes only partly (2−5 times) to the faster fibril formation at this tip. An additional speed-up comes about since during subsequent structural reorganization of the monomer, the exposed F19 at the even tip

can form transient interactions with parts of the monomer when its compact structures are disrupted. Such interactions are absent at the odd tip. Taken together, we suggest that the even tip with the exposed CHC region, and thus exposed F19, serves as a better template to catalyze fast fibril formation than does the odd tip.

■ METHODS

PACE Models for Simulation of Aβ. In the present study, we employed a hybrid-resolution model, namely, PACE (available at www.ks.uiuc.edu/∼whan/PACE/PACEvdw/),[44] to simulate Aβ fibril elongation. PACE's parametrization and application to protein folding have been discussed in detail in previous studies.[44,45,48] In the present study, we demonstrate, as shown in SI and Figure S6 (SI), that simulations of A$\beta_{1-40/1-42}$ with PACE reproduce key experimental observables of Aβ structures, including secondary structure content[70] and $^3J_{HNH_\alpha}$ coupling constants measured in NMR experiments,[26] with an accuracy rivaling that of all-atom simulations.[26] Thus, PACE can also be extended to simulations of disordered peptides like Aβ.

Beside Aβ monomer conformational features, we examined also, as described in Results, the ability of PACE to reproduce important quantities relevant to fibril elongation such as Aβ binding affinity and activation enthalpy of fibril formation. We notice that although the two quantities are qualitatively reproduced, they are both overestimated in the present study. As these quantities are determined mainly by HB interactions, we suspect that the PACE force field applied here slightly overestimates individual HB interactions and that the overestimate accumulates for fibril formation in which multiple HB interactions are involved.

Models and Simulation Setup. We built an initial fibril model based on a part of the fibril structure reported by Lührs et al. (PDB ID: 2BEG)[21] containing four Aβ_{17-42} peptides. L17 of Aβ_{17-42} was capped with an acetyl group. The initial model had its fibril axis aligned to the z-direction, and then was solvated in a box of MARTINI water and neutralized with 0.15 M NaCl solution, leading to a system of ∼3000 particles. The system was energy minimized for 5000 steps. The resulting structure was used to prepare starting conformations of incoming monomers and fibrils for production runs in two approaches. In a first approach, the monomer on either accessible edge of fibrils was pulled away from the remaining three, which are positionally fixed, at a speed of 0.25 Å /ns by applying a force in the z-direction to the center-of-mass (COM); the force was generated by pulling the end of an attached spring with spring constant k = 2.4 kcal/mol Å^2, a standard procedure in steered molecular dynamics.[71] In a second approach, we replaced the edge monomer with one randomly selected from a REMD simulation of Aβ_{17-42} (see SI). The selected conformation was randomly placed and oriented.

In the production runs, we performed umbrella sampling simulations with 17 windows whose z-COM distances ranged from 4.8 to 20.8 Å at 1 Å intervals. In each window, a harmonic potential with a force constant of 2.4 kcal/mol Å^2 was applied to maintain the respective z-COM distance. Also, positional restraints were applied to backbone atoms of the three peptides representing fibril tips and their side-chain atoms sandwiched by the two β-sheets of fibrils. The force constant for the positional constraints was 2.4 kcal/mol Å^2. For each window a REMD simulation was performed with 64 NVT replicas at temperatures chosen in the range of 320−650 K. The starting structures for one-half of the replicas were selected from the first approach as discussed above; those for the other half were selected from the second approach. The time step of simulation was chosen to be 4 fs, a value typical for PACE simulations.[45] Exchanges between replicas were attempted every 8 ps and the acceptance ratio was 40−50%. Each replica ran for 0.6 μs and only the last 0.4 μs of simulation was used for analysis. The convergence of sampling is discussed in SI (see Figure S7 (SI)). In addition to the biased simulations, we also performed 480 100 ns unbiased simulations of the association of Aβ with fibrils. The starting structures of these simulations were generated in the second approach and placed halfway between the two fibril tips

under periodic boundary conditions. All simulations discussed above were performed using NAMD 2.9.[72]

Previous REMD simulations with Aβ monomers moving freely have shown that Aβ can not only bind to fibril tips, but can also bind, though with a much smaller affinity, to fibril sides.[39] However, due to the restraints applied in our umbrella sampling simulations, we were unable to observe the weaker binding of Aβ to fibril sides. Consequently, the kinetic network model built upon the simulation results (see below) does not consider the binding to fibril sides as a part of fibril elongation.

Analysis of Transition Kinetics Based on Kinetic Network Model. A class of methods have been developed recently for the study of long-time conformational transitions of proteins through MD simulations.[73,74] These methods are based on kinetic network models which assume that conformational space can be discretized into states and that conformational transitions correspond to hopping of systems between the states. To determine pathways of Aβ structural transitions, we employed one variant of these methods which had been applied successfully to produce plausible pathways for both protein folding and large conformational change of proteins.[50,51,75,76] In this method, kinetic network models are constructed on the basis of states sampled in biased simulations which allow a better sampling of conformations in transition regions that are usually high in energy and, thereby, rarely accessible in unbiased simulations.[50,51,75,76] The detail of the method is described in SI. Briefly, all sampled conformations are first clustered into microstates, employing principal components to measure structural similarity between conformations.[50] The statistical probability of the microstates are then recovered from biased simulations through the T-WHAM method.[59] Connectivity between these microstates is further established assuming that transitions arise between microstates with similar structures.[50,51,75,76] The kinetic rates k_{ij} of transition from connected microstates j to i were assigned as[50,51]

$$k_{ij} = \begin{cases} k_0 & \text{if } p_{eq}(j) \leq p_{eq}(i) \\ \dfrac{p_{eq}(i)}{p_{eq}(j)} k_0 & \text{if } p_{eq}(j) > p_{eq}(i) \end{cases} \quad (2)$$

where $p_{eq}(j)$ is the equilibrium probability of microstate j and k_0 is a base rate constant assumed to be the same for transitions involving any pair of microstates.[50,51] Eq 2 ensures that the detailed balance condition is satisfied in the network. Two important parameters are needed for construction of kinetic network models as described above, namely, a cutoff distance for clustering conformations and a cutoff distance for establishing connectivity between states; in the present study, the two cutoff distances are 2.5 and 3.0 Å, respectively. We also examined, as explained in SI and Figure S8 (SI), other choices for these parameters and demonstrated that key observations of fibril elongation in the present study are not sensitive to the cutoff parameters selected.

According to transition path theory (TPT),[52,53,77] a kinetic network $\{k_{ij}\}$ can be used to investigate transitions between two groups of microstates A and B by determining first the reactive flux J_{ji} from microstates i to j, defined as the net contribution to $A \rightarrow B$ transitions via the transitions between the two microstates. J_{ji} is calculated according to the equation

$$J_{ji} = k_{ji} p_{eq}(i)[p_{fold}(j) - p_{fold}(i)], \ p_{fold}(j) > p_{fold}(i) \quad (3)$$

where $p_{fold}(i)$ is the committor probability of state i, defined as the probability that the system, when being in state i, hits group B states before reaching group A states.[78] The calculation of $p_{fold}(i)$ is described in SI. Using an iterative algorithm from TPT,[53] the network $\{J_{ij}\}$ of reactive fluxes can be decomposed into individual pathways ranked by their fluxes. Many important kinetic properties can be derived according to the calculated network $\{J_{ij}\}$ and the pathways identified, including the macroscopic rate of the $A \rightarrow B$ transition, the probability of a particular pathway to be taken (p_{path}) and the probability of a microstate participating in any of the reactive pathways (p_{onpath}).[53] The TPT analysis on kinetic network models is explained in detail in SI.

■ ASSOCIATED CONTENT

ⓢ Supporting Information

Representative pathway involving antiparallel β-sheet in the CHC region (Figure S1), representative structures of unbound monomers (Figure S2) and monomers involving strand–loop–strand structures (Figure S3), representative (Figure S4) and simplified pathways (Figure S5) of fibril formation at the odd tip, comparison of $^3J_{HNH_\alpha}$ constants between experiments and simulations (Figure S6), analysis of overlap between umbrella sampling windows and variation of simulation temperature and end-to-end distance of Aβ observed in REMD simulations (Figure S7), representative fibril formation pathways obtained with different cutoff parameters (Figure S8), schemes of structural models of β-sheet and strand–loop–strand structures (Figures S9–10), discussions on applicability of PACE to Aβ simulations and on convergence of sampling, detail of kinetic network analysis, secondary structure analysis, analysis of strand–loop–strand structures and estimation of binding affinity. This material is available free of charge via the Internet at http://pubs.acs.org.

■ AUTHOR INFORMATION

Corresponding Author

kschulte@ks.uiuc.edu

Notes

The authors declare no competing financial interest.

■ ACKNOWLEDGMENTS

■ REFERENCES

(1) De Strooper, B. *Physiol. Rev.* **2010**, *90*, 465−494.

(2) Holtzman, D. M.; Morris, J. C.; Goate, A. M. *Sci. Transl. Med.* **2011**, *3*, 77sr1−77sr1.

(3) Yankner, B. A.; Lu, T. *J. Biol. Chem.* **2009**, *284*, 4755−4759.

(4) Petkova, A. T.; Leapman, R. D.; Guo, Z.; Yau, W.-M.; Mattson, M. P.; Tycko, R. *Science* **2005**, *307*, 262−265.

(5) Qiang, W.; Yau, W.-M.; Luo, Y.; Mattson, M. P.; Tycko, R. *Proc. Natl. Acad. Sci. U. S. A.* **2012**, *109*, 4443−4448.

(6) Walsh, D. M.; Hartley, D. M.; Kusumoto, Y.; Fezoui, Y.; Condron, M. M.; Lomakin, A.; Benedek, G. B.; Selkoe, D. J.; Teplow, D. B. *J. Biol. Chem.* **1999**, *274*, 25945−25952.

(7) Chimon, S.; Shaibat, M. A.; Jones, C. R.; Calero, D. C.; Aizezi, B.; Ishii, Y. *Nat. Struct. Mol. Biol.* **2007**, *14*, 1157−1164.

(8) Lu, J.-X.; Qiang, W.; Yau, W.-M.; Schwieters, C. D.; Meredith, S. C.; Tycko, R. *Cell* **2013**, *154*, 1257−1268.

(9) Reinke, A. A.; Gestwicki, J. E. *Chem. Biol. Drug Des.* **2007**, *70*, 206−215.

(10) Härd, T.; Lendel, C. *J. Mol. Biol.* **2012**, *421*, 441−465.

(11) Wetzel, R. *Acc. Chem. Res.* **2006**, *39*, 671−679.

(12) Kusumoto, Y.; Lomakin, A.; Teplow, D. B.; Benedek, G. B. *Proc. Natl. Acad. Sci. U. S. A.* **1998**, *95*, 12277−12282.

(13) Esler, W. P.; Stimson, E. R.; Jennings, J. M.; Vinters, H. V.; Ghilardi, J. R.; Lee, J. P.; Mantyh, P. W.; Maggio, J. E. *Biochemistry* **2000**, *39*, 6288−6295.

(14) Cannon, M. J.; Williams, A. D.; Wetzel, R.; Myszka, D. G. *Anal. Biochem.* **2004**, *328*, 67−75.

(15) O'Nuallain, B.; Shivaprasad, S.; Kheterpal, I.; Wetzel, R. *Biochemistry* **2005**, *44*, 12709−12718.

(16) Ban, T.; Yamaguchi, K.; Goto, Y. *Acc. Chem. Res.* **2006**, *39*, 663−670.

(17) Buell, A. K.; Dhulesia, A.; White, D. A.; Knowles, T. P.; Dobson, C. M.; Welland, M. E. *Angew. Chem., Int. Ed.* **2012**, *51*, 5247−5251.

(18) Qiang, W.; Kelley, K.; Tycko, R. *J. Am. Chem. Soc.* **2013**, *135*, 6860−6871.

(19) Cohen, S. I.; Linse, S.; Luheshi, L. M.; Hellstrand, E.; White, D. A.; Rajah, L.; Otzen, D. E.; Vendruscolo, M.; Dobson, C. M.; Knowles, T. P. *Proc. Natl. Acad. Sci. U. S. A.* **2013**, *110*, 9758−9763.

(20) Petkova, A. T.; Ishii, Y.; Balbach, J. J.; Antzutkin, O. N.; Leapman, R. D.; Delaglio, F.; Tycko, R. *Proc. Natl. Acad. Sci. U. S. A.* **2002**, *99*, 16742−16747.

(21) Lührs, T.; Ritter, C.; Adrian, M.; Riek-Loher, D.; Bohrmann, B.; Döbeli, H.; Schubert, D.; Riek, R. *Proc. Natl. Acad. Sci. U. S. A.* **2005**, *102*, 17342−17347.

(22) Petkova, A. T.; Yau, W.-M.; Tycko, R. *Biochemistry* **2006**, *45*, 498−512.

(23) Ma, B.; Nussinov, R. *Curr. Opin. Chem. Biol.* **2006**, *10*, 445−452.

(24) Miller, Y.; Ma, B.; Nussinov, R. *Chem. Rev.* **2010**, *110*, 4820−4838.

(25) Zhang, S.; Iwata, K.; Lachenmann, M.; Peng, J.; Li, S.; Stimson, E.; Lu, Y.-A.; Felix, A.; Maggio, J.; Lee, J. *J. Struct. Biol.* **2000**, *130*, 130−141.

(26) Sgourakis, N. G.; Yan, Y.; McCallum, S. A.; Wang, C.; Garcia, A. E. *J. Mol. Biol.* **2007**, *368*, 1448−1457.

(27) Ball, K. A.; Phillips, A. H.; Nerenberg, P. S.; Fawzi, N. L.; Wemmer, D. E.; Head-Gordon, T. *Biochemistry* **2011**, *50*, 7612−7628.

(28) Ball, K.; Phillips, A. H.; Wemmer, D. E.; Head-Gordon, T. *Biophys. J.* **2013**, *104*, 2714−2724.

(29) Lam, A.; Rodriguez, J.; Rojas, A.; Scheraga, H.; Mukamel, S. *J. Phys. Chem. A* **2013**, *117*, 342−350.

(30) Straub, J. E.; Thirumalai, D. *Annu. Rev. Phys. Chem.* **2011**, *62*, 437−463.

(31) Massi, F.; Straub, J. E. *Proteins: Struct., Funct., Bioinf.* **2001**, *42*, 217−229.

(32) Li, M. S.; Klimov, D.; Straub, J.; Thirumalai, D. *J. Chem. Phys.* **2008**, *129*, 175101.

(33) Santini, S.; Mousseau, N.; Derreumaux, P. *J. Am. Chem. Soc.* **2004**, *126*, 11509−11516.

(34) Nguyen, P. H.; Li, M. S.; Stock, G.; Straub, J. E.; Thirumalai, D. *Proc. Natl. Acad. Sci. U. S. A.* **2007**, *104*, 111−116.

(35) Baumketner, A.; Krone, M. G.; Shea, J.-E. *Proc. Natl. Acad. Sci. U. S. A.* **2008**, *105*, 6027−6032.

(36) Reddy, G.; Straub, J. E.; Thirumalai, D. *Proc. Natl. Acad. Sci. U. S. A.* **2009**, *106*, 11948−11953.

(37) O'Brien, E. P.; Okamoto, Y.; Straub, J. E.; Brooks, B. R.; Thirumalai, D. *J. Phys. Chem. B* **2009**, *113*, 14421−14430.

(38) Takeda, T.; Klimov, D. K. *Biophys. J.* **2009**, *96*, 4428−4437.

(39) Takeda, T.; Klimov, D. K. *Biophys. J.* **2009**, *96*, 442−452.

(40) Fawzi, N. L.; Okabe, Y.; Yap, E.-H.; Head-Gordon, T. *J. Mol. Biol.* **2007**, *365*, 535−550.

(41) Rojas, A.; Liwo, A.; Browne, D.; Scheraga, H. A. *J. Mol. Biol.* **2010**, *404*, 537−552.

(42) Ban, T.; Hoshino, M.; Takahashi, S.; Hamada, D.; Hasegawa, K.; Naiki, H.; Goto, Y. *J. Mol. Biol.* **2004**, *344*, 757−767.

(43) Kellermayer, M. S.; Karsai, Á.; Benke, M.; Soós, K.; Penke, B. *Proc. Natl. Acad. Sci. U. S. A.* **2008**, *105*, 141−144.

(44) Han, W.; Wan, C.-K.; Jiang, F.; Wu, Y.-D. *J. Chem. Theory Comput.* **2010**, *6*, 3373−3389.

(45) Han, W.; Schulten, K. *J. Chem. Theory Comput.* **2012**, *8*, 4413−4424.

(46) Marrink, S. J.; Risselada, H. J.; Yefimov, S.; Tieleman, D. P.; de Vries, A. H. *J. Phys. Chem. B* **2007**, *111*, 7812−7824.

(47) Han, W.; Wan, C.-K.; Wu, Y.-D. *J. Chem. Theory Comput.* **2010**, *6*, 3390−3402.

(48) Han, W.; Schulten, K. *J. Phys. Chem. B* **2013**, *117*, 13367−13377.

(49) Chen, J. *J. Am. Chem. Soc.* **2009**, *131*, 2088−2089.

(50) Zheng, W.; Gallicchio, E.; Deng, N.; Andrec, M.; Levy, R. M. *J. Phys. Chem. B* **2011**, *115*, 1512−1523.

(51) Deng, N.-j.; Zheng, W.; Gallicchio, E.; Levy, R. M. *J. Am. Chem. Soc.* **2011**, *133*, 9387−9394.

(52) Berezhkovskii, A.; Hummer, G.; Szabo, A. *J. Chem. Phys.* **2009**, *130*, 205102.

(53) Noé, F.; Schütte, C.; Vanden-Eijnden, E.; Reich, L.; Weikl, T. R. *Proc. Natl. Acad. Sci. U. S. A.* **2009**, *106*, 19011−19016.

(54) Han, W.; Wu, Y.-D. *J. Am. Chem. Soc.* **2005**, *127*, 15408−15416.

(55) Tarus, B.; Straub, J. E.; Thirumalai, D. *J. Am. Chem. Soc.* **2006**, *128*, 16159−16168.

(56) Rosenman, D. J.; Connors, C. R.; Chen, W.; Wang, C.; García, A. E. *J. Mol. Biol.* **2013**, *425*, 3338−3359.

(57) Dovidchenko, N.; Galzitskaya, O. *Biochemistry (Moscow)* **2011**, *76*, 366−373.

(58) Schmit, J. D. *J. Chem. Phys.* **2013**, *138*, 185102.

(59) Gallicchio, E.; Andrec, M.; Felts, A. K.; Levy, R. M. *J. Phys. Chem. B* **2005**, *109*, 6722−6731.

(60) Hwang, W.; Zhang, S.; Kamm, R. D.; Karplus, M. *Proc. Natl. Acad. Sci. U. S. A.* **2004**, *101*, 12916−12921.

(61) Yang, M.; Teplow, D. B. *J. Mol. Biol.* **2008**, *384*, 450−464.

(62) Hoyer, W.; Grönwall, C.; Jonsson, A.; Ståhl, S.; Härd, T. *Proc. Natl. Acad. Sci. U. S. A.* **2008**, *105*, 5099−5104.

(63) Buchete, N.-V.; Hummer, G. *J. Phys. Chem. B* **2008**, *112*, 6057−6069.

(64) Han, W.; Wu, Y.-D. *Proteins* **2007**, *66*, 575−587.

(65) Masman, M. F.; Eisel, U. L.; Csizmadia, I. G.; Penke, B.; Enriz, R. D.; Marrink, S. J.; Luiten, P. G. *J. Phys. Chem. B* **2009**, *113*, 11710−11719.

(66) Lazo, N. D.; Grant, M. A.; Condron, M. C.; Rigby, A. C.; Teplow, D. B. *Protein Sci.* **2005**, *14*, 1581−1596.

(67) Baumketner, A.; Shea, J.-E. *J. Mol. Biol.* **2007**, *366*, 275−285.

(68) Sandberg, A.; et al. *Proc. Natl. Acad. Sci. U. S. A.* **2010**, *107*, 15595−15600.

(69) Larini, L.; Shea, J.-E. *Biophys. J.* **2012**, *103*, 576−586.

(70) Kirkitadze, M. D.; Condron, M. M.; Teplow, D. B. *J. Mol. Biol.* **2001**, *312*, 1103−1119.

(71) Lu, H.; Isralewitz, B.; Krammer, A.; Vogel, V.; Schulten, K. *Biophys. J.* **1998**, *75*, 662−671.

(72) Phillips, J. C.; Braun, R.; Wang, W.; Gumbart, J.; Tajkhorshid, E.; Villa, E.; Chipot, C.; Skeel, R. D.; Kale, L.; Schulten, K. *J. Comput. Chem.* **2005**, *26*, 1781−1802.

(73) Chodera, J. D.; Singhal, N.; Pande, V. S.; Dill, K. A.; Swope, W. C. *J. Chem. Phys.* **2007**, *126*, 155101.

(74) Noé, F.; Fischer, S. *Curr. Opin. Struct. Biol.* **2008**, *18*, 154−162.

(75) Andrec, M.; Felts, A. K.; Gallicchio, E.; Levy, R. M. *Proc. Natl. Acad. Sci. U. S. A.* **2005**, *102*, 6801−6806.

(76) Zheng, W.; Andrec, M.; Gallicchio, E.; Levy, R. M. *J. Phys. Chem. B* **2009**, *113*, 11702−11709.

(77) Metzner, P.; Schütte, C.; Vanden-Eijnden, E. *Multiscale Model. Simul.* **2009**, *7*, 1192−1219.

(78) Du, R.; Pande, V. S.; Grosberg, A. Y.; Tanaka, T.; Shakhnovich, E. S. *J. Chem. Phys.* **1998**, *108*, 334.